

Chapter 5

Conductance-Based Models for the Evaluation of Brain Functions, Disorders, and Drug Effects

Svetlana Postnova, Christian Finke, Martin T. Huber, Karl Voigt
and Hans A. Braun

In order for a mathematical model of a biomedical system to be valuable for experimental and clinical research it must be designed in accordance with the experimental or clinical problem.

5.1 Introduction

Neurological and psychiatric disorders such as Parkinson's disease and clinical depression are both diseases of the nervous system. Disorders of different autonomic functions, including disturbances of sleep, energy balance, and hormonal secretion also have their origin in brain dysfunctions. However, while diseases associated with energy control or hormonal secretion can be diagnosed by measuring specific parameters (so-called biomarkers) such as blood glucose or hormone concentration, diagnosis is much more difficult for psychiatric disorders such as clinical depression or manic-depressive states, also known as unipolar and bipolar disorders.

Many of the neurological diseases can be attributed to specific dysfunctions, e.g. in the dopamine system for Parkinson's disease, or the destruction of cholinergic receptors at the motor endplate in the case of Myasthenia gravis (pseudo paralysis, [11]). For sleep disorders and for clinical depression and manic-depressive states on the other hand there are no specific biomarkers on which diagnosis and treatment can rely. The disorders manifest in the patient's clinical psychopathology and, although attempts are being made to correlate different forms of depression with over- or under-expression of particular genes, the diagnosis is essentially based on the doctor's impression of the patient, statements by persons related to the patient, and answers to standardized questionnaires [10].

An additional problem in the treatment of psychiatric disorders is obviously that, while the disease manifests in the patient's behavior, the pharmaceutical treatment interferes with cellular and subcellular mechanisms at the level of ion channels, transporters and genes. Figure 5.1A illustrates the different functional levels that need to be brought together to achieve an understanding of these diseases that can serve as the basis for a rational treatment:

Alteration of a single process at the cellular or subcellular level, by spontaneous malfunction or due to the action of a drug, can drastically change the intra-cellular dynamics. This, in turn, can significantly alter the excitability and sensitivity of in-

dividual neurons, thereby also changing the activity of neuronal networks. This may again have consequences for the functionality of specific brain areas which finally can lead to changes in sensory or motor functions, emotions, mood, or behavior. Moreover, since psychiatric disorders may originate in external circumstances, the proper understanding also requires insights into the inverse causation cascade.

In addition, at all of these vertical levels there is a wide range of systemic interactions on the horizontal level, e.g., through the multiple interlinked second messenger pathways, through the mutual interactions between ion channels, and via the signal transmissions between individual neurons. These horizontal interdependences are illustrated in Fig. 5.1B where we have drawn the connections among some of the different brain areas involved in the regulation of sleep. Even such a simple diagram demonstrates that it is not sufficient to understand how changes on the cellular or subcellular levels affect the functioning of a specific brain area, because the changes will spread to and affect the function of other brain areas as well.

This fantastic interconnectedness serves to make neuronal systems flexible and adaptive on one hand and robust and self-maintaining on the other. At the same time, this interconnectedness is an essential precondition for the enormous information handling capacity of the brain. However, this interconnectedness also contributes to making psychiatric diseases exceedingly difficult to understand and model. Despite all its qualities, the human brain soon reaches its limits in attempts to overlook even a comparatively simple system, particularly if this system includes feedback mechanisms with delays, instabilities and nonlinear dynamic phenomena.

The purpose of this chapter is to discuss different approaches to neuronal modeling and their physiological rationale. The so-called conductance-based approach will be highlighted as a method that allows mathematical models to be developed in close agreement with the underlying physiological mechanisms. With this approach we can start to examine the causes of diseases and the action of drugs in a clinical and pharmacologically relevant perspective. We'll present examples of neuronal dynamics at various levels of the brain, ranging from simulations of individual neurons to complex interactions between different brain areas in the context of the so-called sleep-wake cycle. We'll be particularly interested in discussions of physiologically justified simplifications of the models and of the possibility of extending the models to include different functional levels.

In this context, it is worth emphasizing that the obstacles that prevent a faster progress and a more effective use of mathematical modeling and computer simulations (biosimulation) in the life sciences are related primarily to human communication problems across established disciplinary boundaries. Experimentalists and clinicians often have difficulties in exploiting the fantastic advantages of a mathematical description, while mathematicians, physicist and engineers lack the required understanding of physiological and pharmacological processes as well as of specific problems in experimental and clinical research. Living systems, and particularly of course the brain, represents an enormous challenge to the life sciences, but the challenge to understand such systems is in no way smaller for mathematics and physics.

5.1.1 Modeling Approaches in neuronal dynamics: Problem-Oriented Simulations

The most ambitious modeling approaches attempt to represent the different anatomical levels in full structural and functional detail, the best known example presumably being the 'Blue Brain' project (<http://bluebrain.epfl.ch/>). The goal of this project is to develop a fully realistic model of the brain. Enormous efforts from a large group of scientists have been invested over several years in order to collect all the data necessary to implement such a model on a parallel supercomputer. At the present, the model considers about 200 different types of neurons in the somatosensory cortex, representing the neuronal network of a single neocortical column. Other large-scale modeling efforts are connected with the 'in silicon human' (<http://www.siliconcell.net>) and the 'physiome' (<http://physiome.jp/>) projects. These projects aim to bring together the actually existing, but widely distributed biological knowledge and modeling experience onto a common platform which will allow us to connect the different levels from molecular kinetics to organ functioning [63]. Such projects seem to be directly related with the steadily increasing information exchange via the World Wide Net.

However, the question still remains as to what extent models of psychiatric disorder have to consider the whole spectrum of physiological processes down to the molecular level. This reflects back on the problem we discussed in the first chapters of this book about the purpose of a model. Do we aim for a model that can answer all questions or would it be more rational to aim for a portfolio of models that each can answer a specific set of questions?

Based on the so-called Neuron Field Theory, for instance, mathematical models of functional interactions between different brain areas can successfully be implemented without considering individual action potentials (spikes) and ion currents [52]. (This approach will be discussed in more detail in Chapter 8). Interactions between different brain areas have also been modeled without considering any electrical activity at all, simulating only alterations in the availability of neurotransmitters [50]. Such approaches appear particularly suited in connection with psychiatric disorders that are associated with imbalances among diverse transmitter systems, e.g. with enhanced dopamine levels in schizophrenia [12].

In our point of view, it is not a question whether simplifications should be introduced or not. The question is where and to what extent simplifications can be accepted, or even are necessary to achieve a better insight into the dynamics of essential mechanisms. Indeed, significant understanding of neuronal dynamics has been gained from purely formal models of action potential generation [19, 51, 39, 22]. An example of the use of this type of functional modeling to describe the dynamics of a so-called tripartite system consisting of a pair of pre- and post-synaptic neurons and a glia cell will be discussed in Chapter 6. These examples demonstrate that there is no rule to favor a particular modeling approach over others, but that the approach must depend on the purpose of the study. The present chapter will demonstrate the

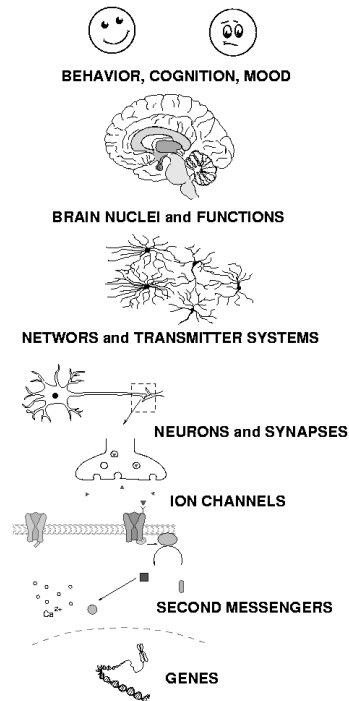
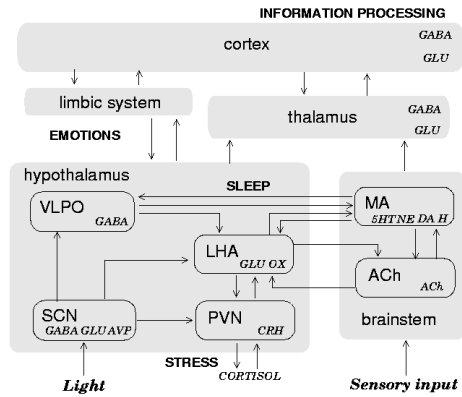
A. Vertical Scale**B. Horizontal Scale**

Fig. 5.1 The vertical scale of different functional levels (A) and the horizontal scale of interacting brain nuclei (B) in the examination of neurological and psychiatric disorders. The vertical scale in A emphasizes the interdependencies among the different functional levels that need to be considered especially in brain-related disorders that are manifested at the behavioural level but most likely originate from disturbances at the cellular and subcellular levels, which are also the main targets for drugs. The horizontal scale in B is illustrated with a selection of brain areas that have to be considered in the context with mental disorders and associated disturbances of autonomic functions, e.g., sleep, emotions, and stress response. The abbreviations are: LHA lateral hypothalamic area; VLPO, SCN, and PVN respectively, are the ventrolateral preoptic, suprachiasmatic, and paraventricular nuclei of the hypothalamus; MA and ACh are the monoaminergic and cholinergic nuclei of the brainstem. The abbreviations in *italics* correspond to a variety of neurotransmitters and hormones that are released by the above brain nuclei for information transmission.

use of a conductance-based approach to examine different physiological processes in neurology and psychiatry.

5.2 Conductance-Based Modeling of Neural Dynamics

The conductance-based approach is used to implement models of neural systems at the level of ion channels (Fig. 5.1). In the field of neurophysiology, such models

are broadly applied for simulation of neurons and synapses. However, the approach allows extensions both towards higher levels of the vertical scale in Fig. 5.1 and to subcellular mechanisms such as second messenger function and gene expression.

In this way, different types of neuronal networks can be designed corresponding to the specific brain areas and functions with physiologically appropriate connections, as illustrated in an example of the horizontal scale in Fig. 5.1B. Similar schemes could be drawn to illustrate horizontal interactions at other levels, not at least for the interaction between different voltage- and transmitter-gated ion channels on which such conductance-based models are built up.

This theoretically describes the general strategy of addressing the challenge of connecting different functional levels and scales. In practice, the realization of such a concept with conductance-based models can easily lead to an overwhelming number of variables and parameters which makes it hard to understand the model's dynamics, and sometimes even prevent elucidation of the physiologically and pathophysiological relevant features.

Our conductance-based models are simplified significantly compared, for example, to the original and widely-used Hodgkin-Huxley approach [23]. However, by contrast to other simplifications, e.g. the FitzHugh-Nagumo model [19], we have specifically made sure that all model variables and parameters retain clear correlations to physiological measures. Our goal is to achieve a physiologically based model structure that allows simplifications and extensions according to the specific task.

In the following sections, we will first describe the physiological background of neuronal excitability and synaptic transmission, and then introduce the general model structure along with examples of how the model equations can be adjusted according to different tasks. These include the elucidation of single neuron dynamics and impulse pattern generation [8, 16, 45], examination of neuronal synchronization [49, 46] and noise effects [18, 17, 44, 26], and the physiologically appropriate implementation of synapses, specifically designed for use in pharmacological and clinical research [45]. Finally, the diverse approaches will be combined in a study of synaptic plasticity in hypothalamic control of sleep-wake cycles with accompanying alterations in thalamic synchronization states [47, 48].

5.2.1 Physiological Background: Basic Membrane Properties

The most relevant structure of information processing in the nervous system is the neuronal membrane and more precisely, the functional proteins that are embedded therein. This is where action potentials, i.e. the major carriers of information to other neurons, are generated, and where the information from other cells is received.

Figure 5.2 illustrates the electrically relevant components. There are ion pumps and ion exchangers (1) to maintain the functionally important concentration differences and to compensate for passive ions fluxes through a diversity of leaky ion channels (2). The multitude of voltage-gated ion channels (3) is represented by two

major types: one having a single gate for channel activation and a second one with an additional gate for inactivation. Typical examples are the Potassium (K) and Sodium (Na) channels for action potential generation.

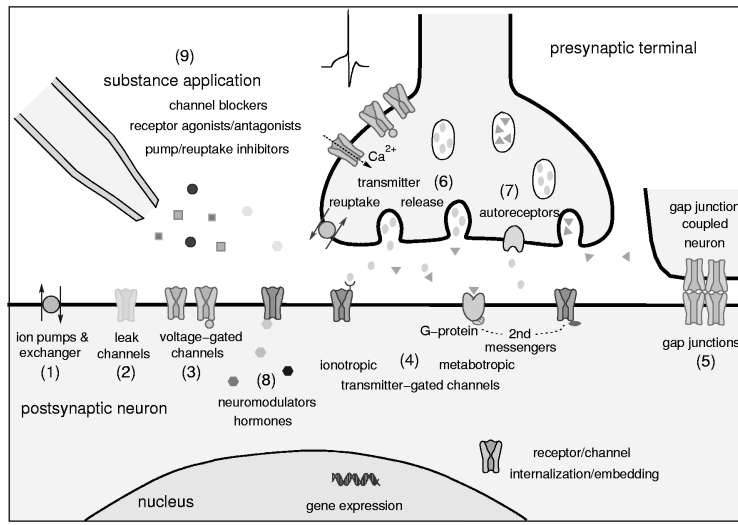


Fig. 5.2 Physiologically relevant processes determining neuronal excitability and synaptic transmission (adapted from [45]). See text for further description.

Transmitter-gated ion channels (4) are combined with a binding site (receptor) for the synaptic transmitter. The receptor can be an integral part of the channel protein directly interfering with its activation state (direct-gating). This is the ionotropic type of synaptic transmission. Other receptors are remote from the ion channels, and are co-localized with G-proteins, which initiate intracellular second messenger cascades to control or modulate the ion channels' state (indirect gating, metabotropic type of transmission). The neurotransmitters are released from presynaptic vesicles (6) into the synaptic cleft. This process is typically initiated by the arrival of an action potential leading to opening of voltage-dependent Ca-channels. The transmitter can control its own release via autoreceptors (7). It can be eliminated via diffusion or degradation and is often actively re-uptaken into the presynaptic terminal. A simpler, electrical, synapse is made up by gap-junctions between neighboring cells (5).

A diversity of neuromodulators and hormones, indicated by floating molecules, interfere with the membrane processes and/or modulates gene expression. Drug application is symbolized by a pipette (9). All membrane proteins are subjected to dynamic control of internalization and degradation or synthesis and embedding. The following discussion specifically addresses generation of impulses by voltage-gated ion channels and their synaptic control, including activity dependent modulation and drug effects.

5.2.2 Modeling Functional Membrane Properties

The principal concept of conductance-based models was developed in the mid-20th century. It was particularly promoted by the work of Hodgkin and Huxley [23], who combined experimental and modeling techniques to explain the appearance of action potentials by voltage- and time-dependent alterations of ionic conductances. Let us start with a short overview of the general idea of a conductance-based approach.

Fig. 5.3 A conductance-based approach. A: The neuronal membrane with voltage- and transmitter-gated ion channels. From left to right: leak channel, voltage-gated potassium and sodium channels, and transmitter-gated channel. B: electrical equivalent circuit corresponding to the membrane and ion channels in A. Adapted from Fig.2 in [45]

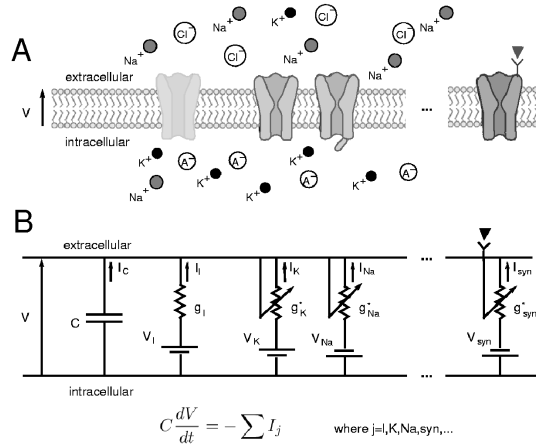


Figure 5.3A presents the dynamically most relevant membrane structures together with their electrical equivalents in Fig. 5.3B. The membrane separates intracellular and extracellular fluids with different ion concentrations which are kept constant by ion pumps (not shown). Electrically, the lipid bilayer can be assumed to be impermeable for ions but it constitutes a capacitor C of significant value (about $1\mu F/cm^2$). Alterations dV/dt of the membrane potential over time are determined by the sum of ion currents ($\sum I$) that are charging the membrane capacitance C :

$$C \frac{dV}{dt} = \sum I \quad (5.1)$$

The ion currents (I) depend on the voltage (V) that drives the ions through the membrane and the electrical resistance (R) which, in physiology, is given by its inverse value, i.e. the electrical conductance, symbolized with a lower case letter g :

$$I = \frac{V}{R} = g \cdot V \quad (5.2)$$

This equation is best known as Ohm's law. However, in the case of neuronal membranes, specific features have to be considered regarding both the conductance and the effective voltage. Physiologically, the actual conductances g_x of specific ion

channels depend on the conductances of single channels ($g_{x,single}$) and the number of open channels ($n_{x,open}$):

$$g_x = n_{x,open} \cdot g_{x,single} \quad (5.3)$$

However, the number of open ion channels cannot be measured directly. It can be estimated from the whole cell currents, if single channel recordings are also being made. Hence, the relevant value, experimentally and in simulations, is the whole cell conductance, conventionally given in relation to a maximum conductance $g_{x,max}$ with a scaling factor a_x , reflecting the portion of opened channels:

$$g_x = a_x \cdot g_{x,max} \quad \text{with} \quad 0 \leq a_x \leq 1 \quad (5.4)$$

Accordingly, equivalent circuits as in Fig. 5.3B do not consider single channels but compound ion currents with all channels of a specific type represented by a single conductance. While the leak conductance can be assumed constant for most situations, those of voltage- and transmitter-gated channels can change and, therefore, are symbolized with sliders.

The equivalent circuit in Fig. 5.3B also contains batteries which do not have direct counterparts in the membrane in Fig. 5.3A. These batteries account for the fact that the voltage driving the ions through the channels is not equal to the membrane potential. Different from technical systems, the reference value for zero current is not the ground potential of 0 mV. Each type of ions has its own potential at which the current is zero. Its value depends on the ion concentrations inside and outside the cell. Due to these concentration differences a chemical gradient drives the ions in the direction of lower concentration, where they produce an electrical field in the opposite direction. The ion flow is zero when the electrical and chemical forces are equal and of opposite direction:

$$z \cdot F \cdot V_{in/out} = -R \cdot T \cdot \ln \left(\frac{C_{in}}{C_{out}} \right), \quad (5.5)$$

where $V_{in/out}$ is the membrane potential measured from the inside to the outside of the cell, C_{in} and C_{out} are the respective ion concentrations, T is the absolute temperature, R is the gas constant, F is Faraday's constant, and z is the valence of the ion. Solving equation (5.5) for V , the equilibrium potential $V_x = V_{in/out}$ for any type of ion x can be calculated:

$$V_x = R \cdot \frac{T}{zF} \cdot \ln \left(\frac{C_{out}}{C_{in}} \right) \quad (5.6)$$

This equation, derived by Walter Nernst already in 1888, is known as the Nernst equation and the equilibrium potentials are called Nernst potentials. These potentials appear in Fig. 5.3B as batteries.

Physiology introduces many complications, including those due to unspecific ion channels. In this case, the voltage of zero current depends on the equilibrium potentials of all the ions that can pass. Electrically, this can be considered as a parallel

circuit with different equilibrium potentials (batteries) and conductances. The common equilibrium potential, i.e. the potential of zero net current flow, is given by

$$V_x = \frac{g_{x1} \cdot V_{x1} + g_{x2} \cdot V_{x2} + g_{x3} \cdot V_{x3} + \dots}{g_{x1} + g_{x2} + g_{x3} + \dots}, \quad (5.7)$$

where x refers to a specific type of ion channel, while $x1, x2, x3, \dots$ represent different ions that can pass with conductance g_{xi} and are driven by equilibrium potentials V_{xi} . In this general form, the potential V_x is called “reversal”, according to observations in electrophysiological experiments that the direction of the ion current is reversed at this point. Note that while the equilibrium potential refers to specific ions and concentration differences, the reversal potential characterizes ion channels.

The reversal potential sets the reference value of zero volt. The effective voltage which is driving the ions through a given type of channels, the so-called “driving force” is given by the distance of the actual membrane potential V to the reversal potential V_x . Ohm’s law, adjusted to ion currents, then has the form

$$I_x = a_x \cdot g_x \cdot (V - V_x) \quad (5.8)$$

For experimental reasons potentials and currents are conventionally given in inside-out direction. In experiments the reference, or ground, electrode is placed in the medium outside the cell while the recording electrode is inserted.

5.2.3 Model Implementation: Simplifications and Extensions

Figure 5.3 illustrates the principle structure of a conductance-based model. In this form it already includes several simplifications. First of all, ion concentrations do not explicitly appear, but only the reversal potentials are given. Furthermore, different ion channels with their conductances and reversal potentials may be combined in one channel type. This is usually the case for the leak channels which all are represented by a single term. If required, the specific types of leak channels or changes of ion concentrations can be included using Eq. (5.7) along with the Eq.(5.6).

Among the most fundamental structures in living systems are active ion pumps which are required to maintain concentration differences. Nevertheless, such pump currents hardly appear in neuronal simulations. Occasionally, an electrogenic component, e.g. of the Na-K pump, is introduced to simulate pump inhibition by cooling or pharmacological substances like heart glycosides [41]. However, if required, the conductance-based approach allows taking into account alterations of ion concentrations due to a possible imbalance of active pump and passive leak currents. It also can consider that the activity of ion pumps, vice versa, depends on the ion concentrations. In the simplest form, this can be introduced by an additional current term that does not depend on the membrane potential or transmitters but on an imbalance between inward and outward currents. There are no limits to implement such interdependences in greater detail, for example, with explicit terms for ion concentrations

according to the Nernst equation and depending on more specific pump currents. Altogether, although the model structure is simplified, it still reflects physiological processes and allows implementing them in more detail whenever requested.

5.3 Neuronal Excitability

The interesting neuronal dynamics arise from ion channels that change their activation state depending on the membrane potential, synaptic transmitters, or other signal substances. Most importantly, neurons can generate so-called action potentials (APs). APs are transient changes of the membrane potential, going from a resting potential, which is near the K-equilibrium, towards the Na-equilibrium potential and back. These types of cells are called “excitable”. In neurons, the APs are fast, spike-like, deflections of the membrane potential.

The mechanisms of neuronal excitability can be looked at from different points of view. In physiological terms we would say that excitability requires “regenerative” or “self-amplifying” processes. From an engineering perspective it can be said that a positive feedback loop is involved. In terms of dynamic systems theory we would say that in response to small disturbance excitable systems show a large deviation from a stable state, which corresponds to a single AP. Despite the difference in terminology all these descriptions of neuronal excitability refer to the same biological phenomenon: the voltage- and time-dependent alterations of ionic conductances.

5.3.1 Voltage-Gated Currents and Action Potentials

In neurons, the regenerative process is constituted by opening of voltage-dependent Na channels in response to depolarization which leads to further depolarization with further opening of Na channels. This would continue until the Na equilibrium potential is reached, if it were not for the opposing effects that are activated almost simultaneously. Firstly, the regenerative process is self-limiting because the Na channels go back to a closed state soon after opening; i.e., they become inactivated. Secondly, with some delay, a negative feedback loop of voltage-dependent K channels is activated driving the membrane potential down towards the K equilibrium potential.

The functional properties of the two major types of ion channels that are responsible for the generation of AP are illustrated in Fig. 5.4 together with the voltage- and time-dependences of their opening and closing. The K channel on the left of Fig. 5.4A represents the simplest type with only one gate (labeled n) which opens on depolarization and closes on repolarisation. The Na channel also possesses such a gate (m), but, there is also a second, the so-called inactivation gate (h), which does just the opposite. It closes on depolarization and opens on repolarisation - luckily with some time delay; otherwise the channel would never be open.

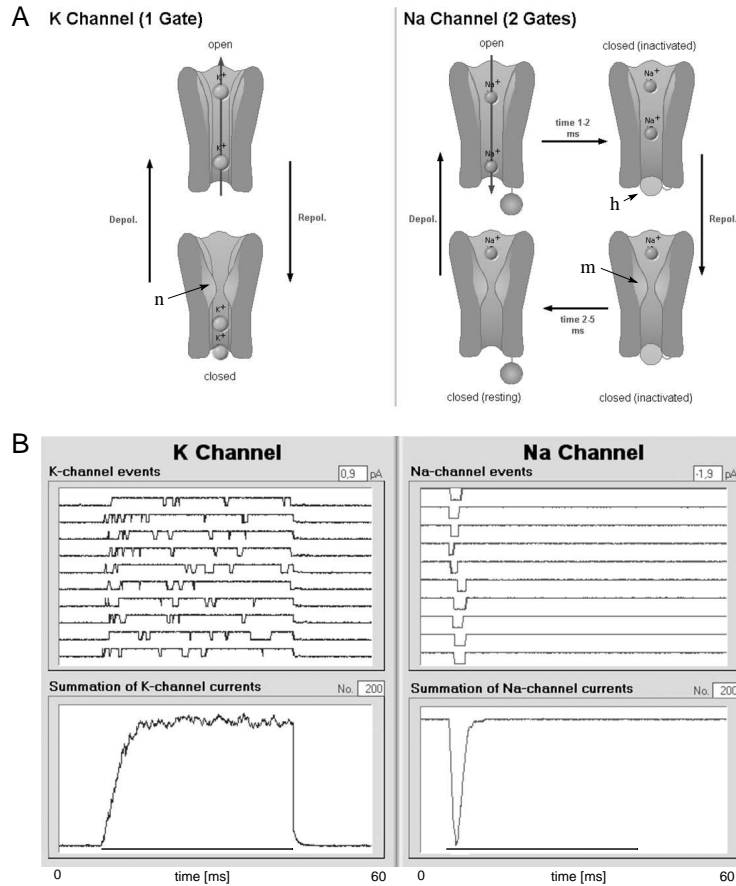


Fig. 5.4 Dynamics of different types of voltage-gated ion channels. A: Ion channels with one and two gates according to the voltage-dependent K^+ and Na^+ channels for action potential generation. B: Opening and closing of K^+ and Na^+ channels in response to a voltage step from -70 to -10 mV (duration indicated by bars at the time axis). The upper traces demonstrate single channel currents on repeated stimulation, and the lower traces show the compound current summed up over 200 recordings. Diagrams and data are from the “cLabs-Neuron” teaching software (www.cLabs.de).

The effects of depolarization on single channel currents are shown in Fig. 5.4B. The upper diagrams show the effects of repeated application of depolarizing voltage steps and illustrate that opening and closing of ion channels are stochastic processes. The single-gate K channel switches randomly between opened and closed states. The double-gated Na channel also opens with random delay and duration. However, this happens only once in response to a depolarizing potential step because the inactivation gate closes, and will only be opened again after repolarisation with significant time-delay of several milliseconds. These are the ionic mechanisms of the refractory period. No Na current will flow as long as the h gate is closed even when a depolarizing stimulus opens the m gate.

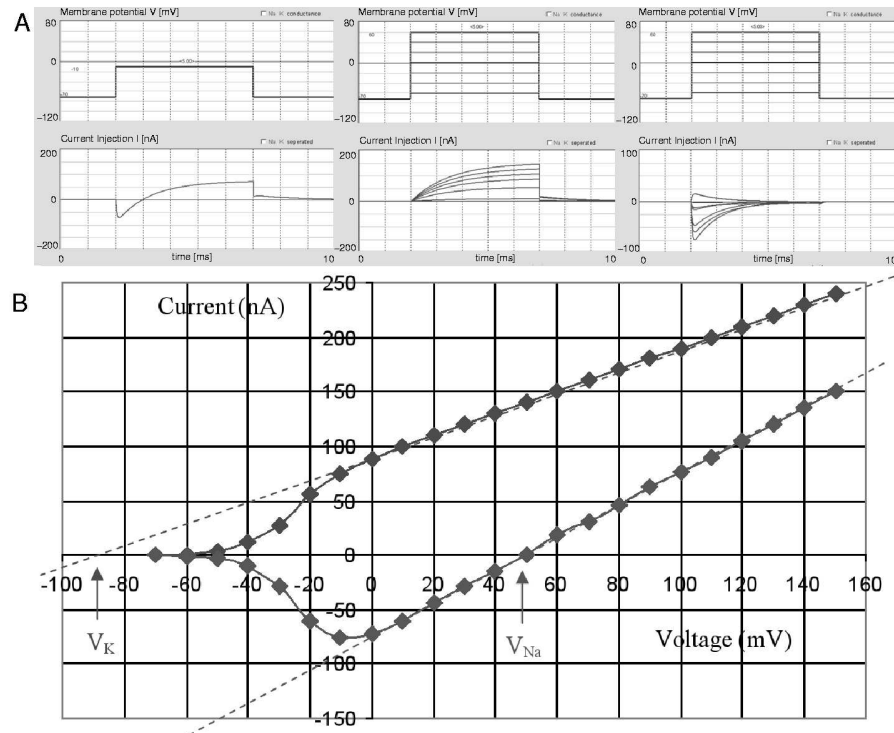


Fig. 5.5 Ion currents and neuronal excitability. A: Virtual voltage-clamp experiments with a model of neuronal excitability. Upper traces demonstrate voltage steps that are applied to the neuron, and lower traces show the resulting ionic currents. Left: Transition from initial Na inward current (downward deflection) to a K outward current in response to a voltage step from -70 to -10 mV. Middle and right diagrams: recordings of isolated K and Na currents when the other current is blocked by TTX or TEA, respectively. Different voltage steps have been applied, as shown in the upper trace. B: Current-voltage (IV) curves of K^+ and Na^+ channels obtained from recordings in the middle and right diagrams in A. Linear IV -relations of constant maximum conductances are indicated by dashed lines and the reversal potentials by arrows. The recordings have been made in the virtual “Voltage- and Current-Clamp Lab” of “cLabs-Neuron” (www.cLabs.de).

Summing up, such single-channel currents generated due to repeated stimulation (Fig. 5.4B, lower diagrams) gives the same curves as would be obtained with whole-cell current recordings to which a manifold of single channels contribute simultaneously (Fig. 5.5A). Such whole-cell experiments need to be done in the voltage/patch-clamp mode. The left diagram shows the overlapping of the fast but transient Na inward with a sustained K outward current in response to a single voltage step. The mid and right diagrams show recordings of isolated K- and Na-currents, respectively, in response to a family of voltage steps from the resting membrane potential to different “command” potentials - a typical experimental procedure.

From the maximum currents of such recordings, current-voltage (I/V) curves can be drawn (Fig. 5.5B). These curves have a linear range with constant conductance (dashed lines) which is achieved when all channels are open. The slope gives the maximum conductance $g = I/V$. Deviations from these curves mean that not all ion channels are opened. The relation between the actual current and the one expected at maximum conductance is used to calculate the voltage-dependent activation state:

$$a_V(V) = \frac{I(V)}{I_{max}(V)} = \frac{g(V)}{g_{max}} \quad (5.9)$$

Typically, the values can be fitted by the Boltzmann function, reflecting a probabilistic distribution of voltage-dependent opening of individual channels with highest transition probabilities around the half-activation potential V_h :

$$a_V(V) = \frac{1}{1 + \exp(-s \cdot (V - V_h))} \quad (5.10)$$

The parameter s is the slope at the half activation potential which determines the broadness of the activation range. The functionally important time delays can be determined from the time course of the current curves as shown in Fig. 5.5A. Mostly, the curves can be fitted quite well by a single exponential function with time constant τ and can be modeled by means of first order differential equation:

$$\frac{da}{dt} = \frac{a_V - a}{\tau} \quad (5.11)$$

Equations (5.10) and (5.11), accounting for voltage and time dependences of ion channels' activation, together with the membrane and current equations (5.1) and (5.8) provide a general and complete set of equations for the development of conductance-based models of neuronal excitability and beyond.

The complete set of equations used to obtain the data in Figs 5.4 and 5.5 is shown in Fig. 5.6. The membrane equation includes, apart from the leak current with constant conductance, the Na and K currents for AP generation with voltage- and time-dependent conductances. Ion currents are given by the product of conductance and driving force. Voltage- and time-dependences of ionic conductances are addressed by activation and inactivation variables (see Fig. 5.4). For AP generation it needs to shift the membrane potential into a voltage range where a sufficient number of Na channels can be opened in order to trigger the regenerative process of depolarization and Na channels activation. All subsequent dynamics are determined by the activation and inactivation processes of the ion channels involved.

5.3.2 Simplifications of the Original Hodgkin-Huxley Equations

The model equations in Fig. 5.6 are significantly simplified compared to the original Hodgkin-Huxley approach [23] that still provides the basis for most conductance-

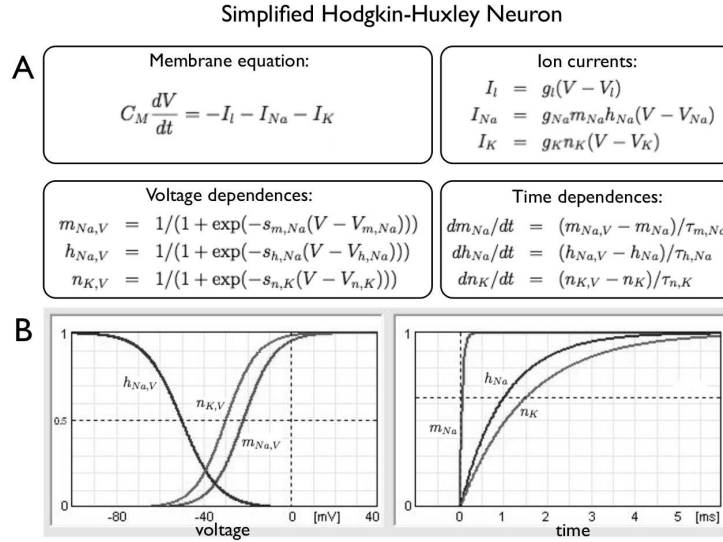


Fig. 5.6 A simplified conductance-based model of Hodgkin-Huxley type. A: the complete set of equations. B: steady-state voltage dependences (left) and time dependences (right) of current activation and inactivation.

based models, not only for neurons but also for other excitable cells as those of the heart. To demonstrate the differences between the original and our simplified approach we refer to an example in Chapter 12 in this book that describes the modeling of cardiac cells. This model is based on the ingenious work of Denis Noble [40] who has adapted the Hodgkin-Huxley (HH) model of nerve excitation for simulation of the pacemaker activity of the heart cells.

The core of all conductance-based models is the membrane equation. Likewise, the diverse ion currents are always calculated as the product of their driving force and ionic conductance. The relevant dynamics are introduced by the voltage and time dependences of the conductances, and exactly these are the points in which the implementations can significantly differ. To illustrate the most important differences between the original and the simplified approach, we compare the calculation of the variable m for Na activation in Fig. 5.7.

In the original HH-equations, all activation variables are determined by exponential rate constants α_m and β_m such as those in equations A1 and A2 of Fig. 5.7, also plotted in insert 1 with numerical values from Surovyatkina (this book). The steady-state voltage-dependencies m_V (A3) as well as the activation time constants τ (A4) are determined to calculate the activation variable m (A5). The exponential rate constants lead to a sigmoid steady state activation curve m_V which appears in the current equation as activation variable m (A6) with the power of 3, thereby adjusted to an appropriate voltage range.

Na-channel activation (m)

A According to the original Hodgkin-Huxley equations:

1. Rate equations:

$$\alpha_m = \frac{100(-V - 48)}{\exp((-V - 48)/5) - 1} \quad (\text{A1})$$

$$\beta_m = \frac{120(V + 8)}{\exp((V + 8)/5) - 1} \quad (\text{A2})$$

2. Steady-state activation:

$$m_V = \frac{\alpha_m}{\alpha_m + \beta_m} \quad (\text{A3})$$

3. Time delay of activation:

$$\tau = \frac{1}{\alpha_m + \beta_m} \quad (\text{A4})$$

4. Activation kinetics:

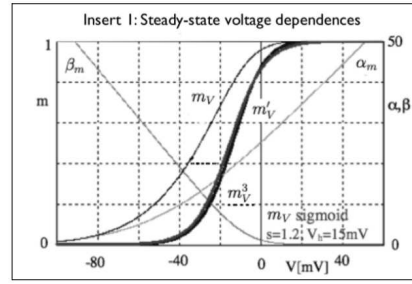
$$\frac{dm}{dt} = \frac{m_V - m}{\tau} \quad (\text{A5})$$

A3/4 combined:

$$\frac{dm}{dt} = \alpha_m(1 - m) + \beta_m m \quad (\text{A5a})$$

5. Current equation:

$$I_{Na} = m^3 \cdot h \cdot g_{Na}(V - V_{Na}) \quad (\text{A6})$$



B Simplified version:

$$m'_V = \frac{1}{1 + \exp(-s(V - V_h))} \quad (\text{B1})$$

$$\frac{dm'}{dt} = \frac{m'_V - m'}{\tau'} \quad (\text{B2})$$

$$I_{Na} = m' \cdot h' \cdot g_{Na}(V - V_{Na}) \quad (\text{B3})$$

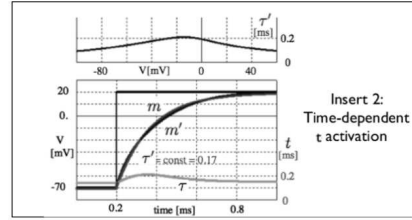


Fig. 5.7 Simplification of the original Hodgkin-Huxley model, demonstrated by means of the Na current activation variable m . A: Equations according to the original Hodgkin-Huxley approach. B: the simplified equations. Inserts 1 and 2 compare voltage and time dependences of the original and simplified model (see text).

Almost identical activation curves can be achieved with a single sigmoid function m'_V (B1), as shown in insert 1 of Fig. 5.7 (curve for m'_V coincides with that for m_V^3). Such form of steady state activation is more appropriate for implementation of m' in the current equation (B3) without the need for a power function. The voltage dependence of the time constant τ , likewise introduced by the rate constants, is plotted in insert 2 of Fig. 5.7. Although τ transiently goes up near the middle of the voltage range (upper trace), the differences in the time-course of m compared to m' with a constant time delay τ' are discernible when plotted over a voltage step that approximately covers the range of an action potential.

The activation variable m is often calculated directly from the time constants, here shown in a form used in Chapter 12. Equations A3 and A4, which here are shown specifically to indicate the physiologically relevant voltage and time dependences, can therefore be skipped. However, the number of equations is not really the problem. Major difficulties for the understanding and adjustment of the dynamics in relation to physiological processes are introduced by the rate constants and power function. What can easily be done with sigmoid activation functions, e.g. accounting

for a shift of the activation range with appropriate adjustment of the half activation voltage V_h , is much more difficult to implement in the rate equations.

In order to understand the reasons for the implementation of rate constants one should remember the situation in the mid-20th century, and especially the challenge that Hodgkin, Huxley, Noble and others have undertaken. The idea to explain the observed dynamics by specific rate transitions has appeared already at that time. Remarkably, all the principle assumptions have been proven to be correct. The ion channel gates, detected in experiments only 25 years later, still are denoted by the letters m , n , and h that Hodgkin and Huxley have introduced. These studies of Hodgkin and Huxley described in their 1952 papers can be considered the most exceptional work in neurophysiology and biophysics in the 20th century. It was done in a combination of electrophysiological experiments and computer modeling studies.

In actual neurophysiology, the focus is not primarily laid on the shape of an AP, although it can still be of interest in case of heart cells. Otherwise, APs are mostly considered in context with the modulation of neuronal firing rates and patterns. Such effects are introduced via the alterations of ionic conductances which are easier to handle with the simplified description. The applied variables and parameters can directly be related to experimental data. From this point of view, the above described simplifications may be considered as adjustments to experimental reality.

A Two-Dimensional Conductance-Based Model of Spike Generation

Real simplifications, including dimension reduction, are implemented with the next steps that eliminate three equations of the already simplified model, two of which are differential (Fig. 5.8). This is achieved by considering activation of Na channels as instantaneous, i.e. without time delays, and neglecting Na channel inactivation.

Neglecting the time delays of Na channel activation is justified because these channels open much faster than any others. Inactivation of Na channels needs to be considered in specific simulations as, for example, voltage-clamp experiments, where it determines the typical time-course of the Na current. In the unclamped, free-running mode of action potentials generation Na channels will anyhow close in the course of K-induced repolarisation. Hence, as long as there is no need to examine some specific phenomena, e.g. in context with a refractory period, the two dimensional model of action potential generation can be used also for extensions in other directions, as described in section 5.5.

A Mathematical Approach: the Two-Dimensional FitzHugh-Nagumo Model

The complicated structure of the original HH equations with four dimensions has challenged many scientists, mostly biophysicists and biochemists, to develop a dimension reduced version of neuronal excitability, especially for explicit analytical examination and easier visualization of the state space dynamics. The most widely

Simplified Hodgkin-Huxley model...

Membrane equation:

$$C_M \frac{dV}{dt} = -I_l - I_{Na} - I_K$$

Ion currents:

$$I_l = g_l(V - V_l)$$

$$I_{Na} = g_{Na} m_{Na} \overline{h_{Na}} (V - V_{Na})$$

$$I_K = g_K n_K (V - V_K)$$

Voltage dependences:

$$m_{Na,V} = 1/(1 + \exp(-s_{m,Na}(V - V_{m,Na})))$$

$$\overline{h_{Na,V}} = 1/(1 + \exp(-s_{h,Na}(V - V_{h,Na})))$$

$$n_{K,V} = 1/(1 + \exp(-s_{n,K}(V - V_{n,K})))$$

Time dependences:

$$\frac{dm_{Na}/dt}{\tau_{m,Na}} = (m_{Na,V} - m_{Na})/\tau_{m,Na}$$

$$\frac{d\overline{h_{Na}}/dt}{\tau_{h,Na}} = (\overline{h_{Na,V}} - \overline{h_{Na}})/\tau_{h,Na}$$

$$\frac{dn_K/dt}{\tau_{n,K}} = (n_{K,V} - n_K)/\tau_{n,K}$$

...reduced to two dimensions

$$C_M \frac{dV}{dt} = -I_l - I_{Na} - I_K$$

$$I_l = g_l(V - V_l)$$

$$I_{Na} = g_{Na} a_{Na}(V - V_{Na})$$

$$I_K = g_K a_K(V - V_K)$$

$$a_{Na,V} = 1/(1 + \exp(-s_{Na}(V - V_{h,Na})))$$

$$a_{K,V} = 1/(1 + \exp(-s_K(V - V_{h,K})))$$

$$da_K/dt = (a_{K,V} - a_K)/\tau_K$$

Fig. 5.8 Reduction of an already simplified four-dimensional Hodgkin-Huxley type model (left) to a two-dimensional version (right). Inactivation of Na -currents (h) is neglected, which makes the calculation of its voltage- and time-dependences dispensable. Considering Na activation as instantaneous eliminates a second differential equation. See text for detail.

used model, which has become a prototype of an excitable neuronal system, was developed by FitzHugh in 1961. This is a two-dimensional system following the equations shown below (see also Postnov et al., this book).

$$\tau_v \cdot \frac{dv}{dt} = v - a \cdot v^3 - b \cdot w + I \quad (5.12)$$

$$\tau_w \cdot \frac{dw}{dt} = v - c \cdot w \quad (5.13)$$

All dynamics are directly related to the main variable v which represents the membrane voltage. Excitation is introduced by a positive feedback from the voltage itself (v), counteracted by a negative feedback loop due to $(-a \cdot v^3)$ and a “recovery” variable (w) which is activated by the voltage (v) with a slower time constant (τ_w), including a relaxation term ($c \cdot w$). A perturbation introduced by the term I can give rise to a spike-like deflection, and a series of spikes can be induced with a firing rate dependent on the strength of I . Moreover, some typical phenomena of neuronal excitability can be observed, e.g. “depolarization block” or “accommodation”.

Dimension reduction from a system theoretical point of view, like the FitzHugh-Nagumo and similar models, can be advantageous for systems analysis but introduces serious limitations when experimentally and clinically relevant mechanisms

need to be examined. For example, electrophysiological experiments are often performed under application of specific ion channel's agonists and antagonists. Also pharmacological treatments of neurological and psychiatric disorders are often interfering with ionic conductances. Under these conditions, conductance-based models have clear advantages. They also can be simplified and reduced in dimensions as shown above. Moreover, if required, physiologically appropriate extensions can be made as we show below.

5.4 Ion Channels and Impulse Patterns

An enormous variety of ion channels can be involved in the control of neuronal excitability. Often, specific functions of a cell are closely related to the expression of specific types of ion channels. In the following we give an example of the development of a single neuron pattern generator which elucidates interesting characteristics that may be of functional relevance for several aspects of neuronal information processing, e.g. sensory information transmission and neuronal synchronization.

The model was originally developed for the simulation of peripheral cold receptor discharges [7]. Cold receptors show the greatest variety of impulse patterns that have been observed in recordings from individual neurons [5]. These include different types of single spike-discharges (tonic firing), impulse groups (bursts), and chaotic pattern [6]. These impulse patterns seem to arise from the interaction between spike generation and subthreshold membrane potential oscillations [8]. Such mechanisms and patterns can not be simulated with a two-dimensional conductance-based model, but requires model extensions.

As experiments suggested the existence of subthreshold oscillations operating independently from spike-generation [5, 54], we have extended the two-dimensional model in Fig. 5.8 by two slow, subthreshold currents I_{ds} and I_{rs} :

$$C \cdot \frac{dV}{dt} = \sum I_M = I_l + I_d + I_r + I_{ds} + I_{rs} \quad (5.14)$$

To underline that this is a generic approach we denote all voltage dependent currents in terms of depolarizing (d) and repolarising (r), with the additional suffix (s) for the slow, subthreshold currents. "Subthreshold" means that these currents are activated below the "threshold" of spike generation, while "slow" refers to the fact that these currents are activated much slower than the spike-generating currents.

We have implemented and used this model in different ways. In its simplest form it is entirely composed of voltage-dependent currents according to the equations in Fig. 5.7B. For slow subthreshold currents the range of voltage-dependent activation is shifted to more negative potentials (subthreshold) and they are activating with significantly larger time constants (slow). Such model simulates the encoding properties of shark electroreceptors and accounts for neuromodulatory properties of brain cells [24]. For the simulation of cold receptor discharges, we had to consider the outcomes of electrophysiological experiments with Ca-channel blockers and changed

Ca-concentrations which indicated significant contribution of Ca-dependent K conductances to impulse pattern generation [55].

Such mechanisms have originally been implemented in all detail with voltage-dependent Ca-currents, alterations of intracellular Ca concentration, and the thereby activated K currents [25]. Later, significant simplifications have been introduced. Activation a_{sr} of the slow repolarising K current has been directly connected to the slow depolarizing current I_{sd} with a coupling factor η , time constant τ_{sr} , and k as a scaling factor of the relaxation term

$$\frac{da_{sr}}{dt} = \frac{\eta \cdot I_{sd} - k \cdot a_{sr}}{\tau_{sr}} \quad (5.15)$$

Temperature dependences have been implemented, according to experimental data, with scaling factors 3.0 and 1.3 per 10°C for all activation time constants and maximum conductances, respectively (see [7, 8] for details and parameter values).

Additionally, noise has been introduced because a specific type of patterns cannot be explained without stochastic components [9, 7, 8]. We have implemented conventional Gaussian white noise in different ways: as current and as conductance noise. The most widely used implementation is additive current noise:

$$C \cdot \frac{dV}{dt} = \sum I_M + I_{Noise} \quad (5.16)$$

Such current noise is assumed to comprise all kinds of random influences, irrespective of their origin. It is an appropriate implementation of synaptic noise and may also reflect environmental fluctuations, e.g., of different neuromodulatory substances. As major noise effects, especially in isolated neurons, may arise from the stochastic opening and closing of ion channels, we have also introduced conductance noise by adding the noise term to the ion channel activation kinetics

$$\frac{da}{dt} = \frac{a_V - a}{\tau} + a_{Noise} \quad (5.17)$$

or, with most dramatic effects, to the Ca-dynamics (according to equation (5.15))

$$\frac{da_{sr}}{dt} = \frac{\eta \cdot I_{sd} - k \cdot a_{sr}}{\tau_{sr}} + a_{Noise} \quad (5.18)$$

The outcomes of the model are shown in Fig. 5.9A by plots of interspike intervals (ISI), which are the time intervals between successive spikes. Figure 5.9B shows examples of voltage traces (for details see [18, 44]). The deterministic bifurcation structure in the upper diagram of Fig. 5.9A demonstrates transitions from tonic firing via chaos to burst discharges and again to tonic firing. In noisy simulations, shown in lower diagrams, these transitions are smeared out. At high temperatures a particular type of pattern appears which does not exist in deterministic simulations. This has been analyzed in detail and is comparably easy to understand [9, 24, 16, 17].

Here, we specifically emphasize the noise effects in the lower temperature range where deterministic simulations exhibit a pacemaker-like tonic firing. Especially

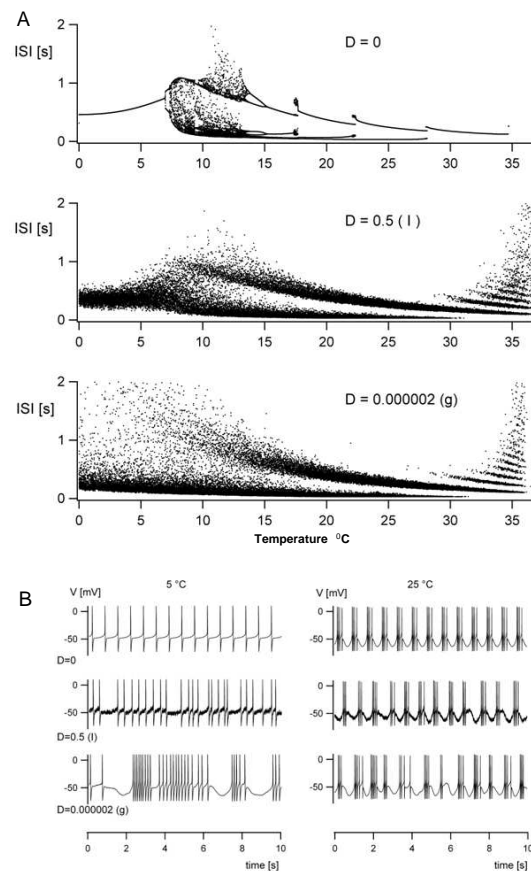


Fig. 5.9 Impulse patterns and effects of current and conductance noise in a model neuron with subthreshold oscillations. A: Bifurcation diagrams of interspike-intervals (ISI) obtained by temperature tuning for the deterministic case (upper diagram), with current noise (mid-diagram), and conductance noise (lower diagram). B: Examples of voltage traces and impulse patterns at 5 and 25 °C of the simulations in A. The values of D give the intensity of Gaussian white noise. The data were presented in an other form in [18, 44]

with application of conductance noise the bursting activity seems to continue far into the deterministically tonic firing regime, but with a more irregular pattern. Examples of voltage traces in Fig. 5.9B additionally underline the noise effects in the tonic firing regime (5°C) in comparison with bursting (25°C) where current as well as conductance noise mainly introduce some randomness in impulse generation.

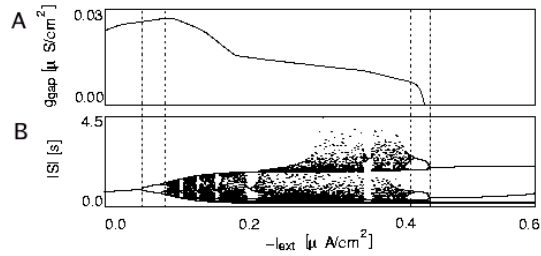
These simulation data suggest that the transitions from pacemaker-like tonic firing to burst discharges via period doubling bifurcation, including a broad range of chaos, are endowed with particularly complex dynamics. These particular dynamics, although not yet fully understood, seem to have significant impact on neuronal synchronization as we illustrate in the next section.

5.5 Gap Junction Coupling and Neuronal Synchronization

Alterations of impulse patterns can be observed not only in recordings from peripheral sensory receptors but also in many neurons in the central nervous system (CNS). Especially the transitions from tonic firing to burst discharges were shown to play a major role in diverse functions, mostly in context with neuronal synchronization. The best known example is synchronization of thalamic and cortical neurons at the transition from wakefulness to sleep which goes along with alterations of neuronal impulse pattern from tonic firing to bursting [32, 35]. Similar interdependences have been suggested to underlie information binding in the visual cortex where synchronization even among distant neurons was observed in parallel with the occurrence of burst discharges [57]. Synchronized neuronal discharges in Parkinson's disease and epilepsy also seem to be associated with transitions to bursting behavior [29, 38]. It is still not clear whether burst activity appears due to neuronal synchronization or neuronal synchronization is a consequence of tonic to bursting transitions.

In order to study synchronization properties at tonic-bursting transition we have used a basic approach of only two neurons connected via gap-junctions (electrotonic or diffusive coupling, for details see [49, 46]). Instead of temperature scaling as in Fig. 5.9 we have used an external current as control parameter which may reflect a compound synaptic input and leads to similar bifurcations (for comparison see Fig. 4 in [44]). Fig. 5.10B shows the transitions from pacemaker-like tonic firing via chaos to bursting that apparently are of particular interest for neuronal synchronization.

Fig. 5.10 Synchronization properties of the gap-junction coupled model neurons. A: Minimal coupling strength g_{gap} required for in-phase synchronization of identical neurons with impulse pattern according to B. Bifurcation diagram of interspike intervals (ISI) obtained by external current injection I_{ext} .



Gap-junction coupling means that individual neurons receive additional currents I_{gap} from their neighboring neurons which depend on the actual potential difference ($V_i - V_j$) and the conductance of the gap-junctions g_{gap} .

$$I_{gap,i} = g_{gap} \cdot (V_i - V_j) \quad \text{with } i, j = 1, 2 \quad (\text{in case of only two neurons}) \quad (5.19)$$

In deterministic simulations, when the two model neurons operate in identical periodic states, they are expected to synchronize even with extremely low coupling strengths, irrespective of their initial conditions. Indeed, this is the case in the bursting regime but, surprisingly, not in the likewise periodic tonic-firing regime. There,

as shown in Fig. 5.10A, the coupling strengths which are needed for in-phase synchronization are even higher than in most ranges of the chaotic regime.

In addition to the above described noise effects, these synchronization data provide further indications that this kind of tonic-firing activity is governed by more complex dynamics than could be expected from a simple pacemaker neuron. Indeed, this tonic activity would not exist without the subthreshold currents, even though the oscillations can no longer be recognized [8]. We will return to the issue in context with a model of hypothalamic control of thalamic synchronization along sleep-wake cycles. This model also includes chemical synapses which are described next.

5.6 Chemical Synapses - the Main Targets of Drugs

The most relevant contacts for specific information transmission, especially over long distances and for communication among brain areas, are made via chemical synapses. In contrast to the electrical synapses, information transmission via chemical synapses is unidirectional. The type of information transmission transiently changes from electrical to chemical. The electrical activity in the presynaptic terminal, mostly in form of action potentials, induces the release of chemical transmitters (also called neurotransmitters) which are modulating the electrical activity of the postsynaptic neuron. This process goes through a number of steps, providing targets for other chemicals, especially drugs. Likewise, many brain disorders are likely to originate from disturbances of chemical information transmission.

Multiple neurotransmitters are present in the brain. Some of them are ubiquitous, like glutamate or gamma-amino-butyric-acid (GABA) which are the major excitatory and inhibitory transmitters. Others, like serotonin, are released by specific, often small brain nuclei, but are involved in the control of a multitude of functions. The cause of neurological and psychiatric diseases is often assumed in an imbalance of diverse transmitter systems, and is modeled accordingly [50, 42]. Most drugs for the treatment of these disorders also interfere with synaptic transmission.

Together with these classical neurotransmitters neurons often release the so-called co-transmitters, which typically are neuropeptides. During recent years a great number of such co-transmitters have been identified, and it can be expected that many more will follow. Action of such co-transmitters is usually not easy to detect in electrophysiological experiments, because they mostly exert neuromodulatory effects and, compared to classical transmitters, do not induce strong potential deflections. Nevertheless, these co-released neuropeptides are involved in a multitude of physiological actions and are becoming increasingly popular for drug development. Activity and effects of such a neuropeptide, i.e. orexin which is required for sustained wakefulness, will be considered in more detail in section 5.8.

5.6.1 A Conductance-Based Model of Synaptic Transmission

In the following a modeling approach is described that does not aim to simulate a specific synapse but should reflect general mechanisms of synaptic transmission. We particularly emphasize the model structure that allows easy adjustments and extensions if specific functions or mechanisms need to be examined in detail.

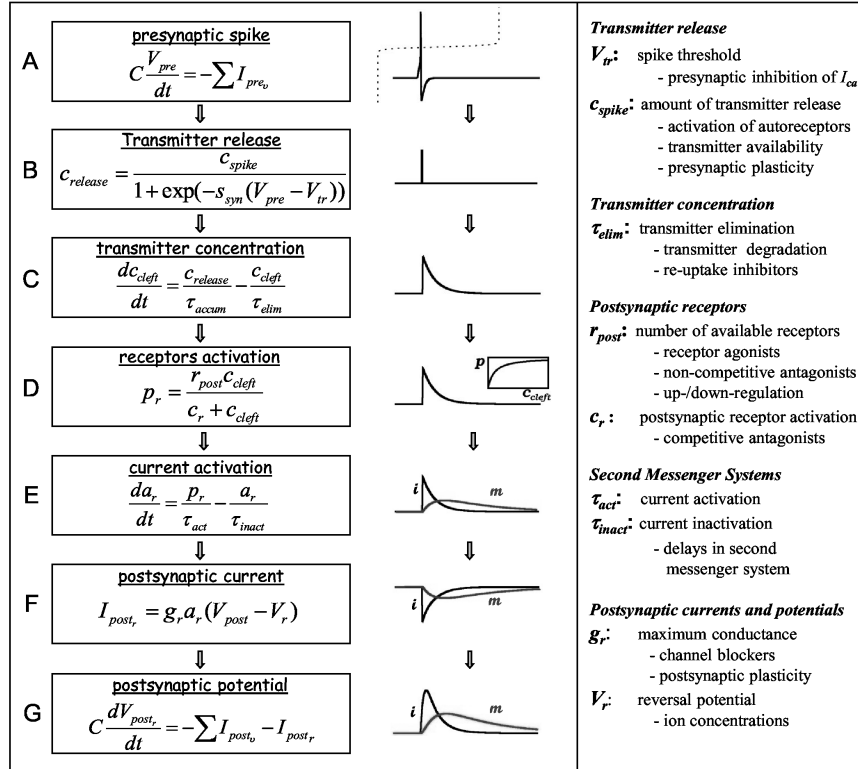


Fig. 5.11 The conductance-based model of synaptic transmission. Equations are given in the left box, together with illustrations of the variables time-course. Main control parameters and their physiological/pharmacological functions are indicated in the box on the right (modified and extended from Fig. 4 in [45]).

Figure 5.11 illustrates the different steps of synaptic transmission and their implementation in the model (for details see [45]). The sequence of synaptic transmission starts with the presynaptic spike (Fig. 5.11A). Release of a neurotransmitter is initiated via the activation of voltage-dependent Ca channels in the membrane of the presynaptic terminal. The increasing concentration of calcium in the terminal activates a sequence of events that leads to the fusion of transmitter-containing vesicles with the presynaptic membrane and subsequent release of transmitter into

the cleft. These mechanisms are not implemented in detail. The steep sigmoid activation function, which is shown with dashed line in Fig. 5.11A, limits the time of transmitter release to the duration of the presynaptic action potential. It is calculated according to equation given in Fig. 5.11B for $s_{syn} = 1$, $V_{tr} = -30mV$. The amount of transmitter being released is adjusted by the scaling factor c_{spike} .

The time delays of transmitter release, including accumulation and elimination of calcium in the presynaptic terminal, as well as vesicle fusion, are very short. Therefore, they can be comprised in the time delays of transmitter accumulation (τ_{accum}) and elimination (τ_{elim}) in equation in Fig. 5.11C, which calculates the time course of transmitter concentration in the cleft. Transmitter elimination is implemented in form of a first order relaxation. This process is the slowest when the transmitters are eliminated only by passive diffusion, but can be accelerated by active processes like degradation and/or reuptake of the transmitter to the presynaptic terminal.

Activation of postsynaptic receptors p_r depends on the transmitter concentration in the cleft and on the availability of the receptors on the postsynaptic membrane. This can be modeled in a form of Michaelis-Menten kinetics, as shown in the inset in Fig. 5.11C. The parameter c_r in Fig. 5.11C is the transmitter concentration at which half of the receptors are occupied. Accordingly, this parameter reflects the transmitter's affinity. The value of r_{post} scales the maximum activation which is reached when all receptors are occupied, thereby representing also the availability of receptors. With a single presynaptic spike the transmitter concentration p_r remains far below saturation and its time course is almost the same as of c_{cleft} .

In case of ionotropic receptors, which are an integral part of the ion channels, receptor activation leads to immediate current activation without discernible time delay ($a_r = p_r$ in Fig. 5.11E). The differential equation in Fig. 5.11E is especially introduced to account for the multitude of G-protein coupled, i.e. metabotropic, receptors where the ion channels are remote from the transmitters' binding sites. In this case, ion channel activation and inactivation goes through a diversity of steps. All additional time delays are comprised in time constants of receptors' activation τ_{act} and inactivation τ_{inact} . The time delays of metabotropic receptors' activation and inactivation are much longer than those of ionotropic, as shown in Fig. 5.11E.

Activation of postsynaptic ion channels induces postsynaptic currents which follow the same rules as the voltage-gated ones (see equation in Fig. 5.11F). Finally, in the membrane equation in Fig. 5.11E the synaptic current $I_{post,r}$ is added to the voltage-dependent currents $I_{post,v}$ leading to the appearance of postsynaptic potentials (PSPs) in the voltage trace V_{post} . Additional time delays in the voltage compared to the currents are introduced by the membrane capacitance C_{post} .

Whether a depolarizing or hyperpolarising postsynaptic current is induced, i.e. whether the synapse is excitatory or inhibitory, depends on the type of postsynaptic ion channels, more precisely, on the conductivities and equilibrium potentials of the ions that can pass (see section 5.3). The type of ion channels that are being opened or closed, in turn, depends on the receptors to which the transmitters bind. Moreover, for the same neurotransmitter, different types of receptors exist, e.g., glutamate-activated AMPA and NMDA receptors. Also, different second messenger pathways can be activated, sometimes even with opposite effects as, for example, via D1 and

D2 dopamine receptors. The multitude of receptors and ion channels provides many targets for pharmaceutical interference with synaptic transmission.

5.6.2 Modeling Synaptic Plasticity and Drug Effects

Compared to physiological reality the presented model is extremely simplified and could be further simplified depending on the task. In this form, it includes major parameters for the simulation of synaptic plasticity, synaptic disturbances, and drug effects. Key functions of specific parameters are listed in the text box of Fig. 5.11.

Transmitter Release:

Presynaptic Inhibition, Autoreceptors, Depletion, and Plasticity

Starting at the presynaptic terminal, the first physiologically relevant value for regulation of synaptic transmission is the amount of transmitter being released. The model, even in this simplified form, provides a number of parameters and variables to distinguish between different effects. Among them is the amplitude of the presynaptic action potential, manifested in V_{pre} which can change depending on the presynaptic activity. Physiologically, it is systematically modified via presynaptic inhibition which uses pre-depolarisation for gradual Na-channel inactivation. In the actual model version, such effects would be achieved with addition of an external, pre-depolarizing current to the presynaptic membrane equation.

Another type of presynaptic inhibition acts via the reduction of presynaptic Ca-inflow. This can be modeled with elevation of the threshold V_{tr} or, in a simpler way, with reduction of c_{spike} , which are both shown in Fig. 5.11B. The scaling parameter c_{spike} can also be used to account for presynaptic plasticity or alterations of presynaptic transmitter availability, e.g. on application of monoamino-oxidase (MAO) inhibitors. An important physiological feedback loop for the control of neurotransmitter release is activated via autoreceptors in the presynaptic membrane, as shown in Fig. 5.2. This can be simulated, in a simplified form, with scaling c_{spike} as a function of the transmitter concentration in the synaptic cleft c_{left} .

Transmitter Concentration: Degradation and Re-uptake Inhibitors

The transmitter concentration in the synaptic cleft (c_{left} in Fig. 5.11C) is a key variable of synaptic transmission determining the activation of postsynaptic receptors. The relevant control parameter is the time constant of transmitter elimination τ_{elim} which accounts for diffusion, degradation, and re-uptake. The active processes of degradation and re-uptake are targets of drugs in a multitude of diseases. A good example is treatment of a muscle disease, Myasthenia gravis, with inhibition of acetylcholine degradation [15].

At most synapses, the transmitters are not only degraded but also re-uptaken from the synaptic cleft back into the presynaptic terminal to be recycled for further transmitter release. This is done by specific transport proteins (see Fig. 5.2), which are again targets of drugs for the treatment of various diseases. For example, specific serotonin re-uptake inhibitors (SSRIs) are among the most widely used drugs in major depression [64]. The primary effect is the strengthening of synaptic transmission due to prolonged presence of the transmitters in the cleft. However, also side-effects have to be considered, e.g. stronger activation of autoreceptors and reduced transmitter release. At the postsynaptic site, prolonged occupation of the receptors can lead to their removal from the membrane, i.e. internalization or down-regulation.

Direct drug effects on transmitter degradation or re-uptake can be implemented in the model with adjustment of the time constant of transmitter elimination (τ_{elim} , Fig. 5.11C). An example of how a pathologically reduced number of receptors can be compensated by re-uptake inhibition is given in [45]. Secondary effects on autoreceptors can be mimicked as described above. For down-regulation of postsynaptic receptors, r_{post} needs to be scaled as a function of receptor activation p_r .

Postsynaptic Receptors: Agonists and Antagonists, Up- and Down-Regulation

Postsynaptic receptors, the binding sites of neurotransmitters, are targets for a multitude of drugs acting as receptor agonists or antagonists. The action of receptor agonists can be considered in the model with a corresponding concentration term added to c_{cleft} , also with implementation of specific pharmacodynamics. Competitive receptor antagonists will lead to a concentration- and affinity-dependent shift of the Michaelis-Menten curve to the right (Fig. 5.11D) which can be introduced by increasing c_r . In contrast, non-competitive antagonists do not occupy the binding sites but prevent receptors' activation by prohibiting the necessary conformational changes. Accordingly, their action needs to be considered in a different way; i.e., by a reduction of r_{post} corresponding to the reduced number of receptors that can be activated. The parameter r_{post} can be connected to other physiological and pathophysiological processes, e.g., the above mentioned effects of antagonists and receptor up- and down-regulation.

Second Messenger Systems / Postsynaptic Currents and Potentials

The diversity of second messenger systems is beyond the scope of this chapter. However, adjustment of activation and inactivation time constants (τ_{act} and τ_{inact}) in Fig. 5.11E allows considering alterations of these processes in general form. In case that more detailed simulations need to be implemented, these parameters provide an interface connecting them with the actual model.

For the next steps, from ion channels activation to postsynaptic currents and potentials, the same rules apply as for neuronal excitability in general (see section 5.4). The relevant control parameters are the maximum conductance g_r and the reversal

potential V_r of the ligand-gated ion channels. Additional effects can be introduced via alterations of the membrane potential of the postsynaptic neuron due to internal dynamics and synaptic inputs also from other sources. Short but strong effects appear during action potential generation. An example is given in [44]. Alterations of the driving force can also be induced via the reversal potential V_r as the result of changed ion concentrations and calculated by the Nernst equation (Eq. 5.6).

Scaling the maximum conductance g_r allows to consider alterations of the number of ion channels which can be activated, for example, due to facilitation of NMDA receptor activation and increased conductivity of AMPA receptors in the early and late phase of synaptic plasticity. Furthermore, g_r is a major parameter for implementation of pharmacologically important effects of ion channel blockers.

5.7 Applications: Neurons and Synapses in a Model of Sleep-Wake Regulation

The previous sections have illustrated how neuronal excitability and synaptic transmission can be simulated with a simplified yet flexible conductance-based approach. Let us conclude this chapter by presenting an example of a model system that combines the diverse aforementioned parts for the development of a physiology-based model of sleep-wake regulation. Sleep-wake regulation is a good example showing the challenge introduced by interdependences of physiological processes along the vertical and horizontal scales (see Fig. 5.1).

5.7.1 Sleep-Wake Control: Mechanisms and Models

Several brain nuclei change their activity along the transitions between sleep and wakefulness. These include diverse nuclei in the hypothalamus, brainstem, and the thalamocortical circuit which are all connected to each other creating a complicated system of interdependences as shown in Fig. 5.1B (for review see [53]).

In the hypothalamus, there are at least three nuclei that play a major role in sleep-wake regulation. These are the suprachiasmatic nucleus (SCN), the ventrolateral preoptic hypothalamus (VLPO), and the lateral hypothalamic area (LHA). Neurons in the SCN constitute a master circadian clock which is entrained by the light-dark cycle. By contrast, activity of the VLPO and LHA neurons is state-dependent. VLPO neurons are silent during wakefulness and firing during sleep [56]. Just the opposite is seen in a subpopulation of LHA neurons co-releasing orexin and glutamate. These are silent during sleep but firing during wakefulness [27, 36].

The sleep-wake centers in the hypothalamus are connected to diverse monoaminergic and cholinergic nuclei in the brainstem. These nuclei are involved in the regulation of ultradian rhythms during sleep [33], and provide projections to other brain areas such as the thalamus.

Thalamic neurons, in feedback loops with cortical neurons, show significant changes of impulse patterns and synchronization at sleep-wake transitions [35]. In the wake state, thalamic neurons exhibit unsynchronized tonic firing activity, while they change to synchronized burst discharges during sleep. In this way, the thalamus opens and closes the gate for sensory information transmission to the cortex for conscious perception (e.g. [3]). When the external input is reduced, populations of cortical neurons tend to synchronize as indicated by the appearance of slow wave potentials in the electroencephalogram (EEG) [1, 34].

Different approaches for simulation of sleep-wake transitions can be found in the current literature. Irrespective of how detailed they are, all refer to the generally accepted two-process concept [4] which suggests that sleep-wake transitions are determined by the interaction between a circadian and a homeostatic process. The circadian process can be related to the genetic clock in the SCN [28]. The homeostatic mechanisms are usually attributed to the accumulation and degradation of somnogens, like adenosine, as considered, for example, in the neural field models [43]. A completely different concept proposes sleep-wake dependent synaptic plasticity as a homeostatic mechanism underlying cortical synchronization [61].

Our focus is laid on the recently discovered substance orexin (OX) which is a co-transmitter of only several thousands of neurons in the lateral hypothalamus [59, 62]. Despite their small number, these neurons influence almost the entire brain with densest projections to the brainstem and thalamocortical circuits. It was shown that lack of orexin neurons or reduced availability of orexin itself as well as of its postsynaptic receptors leads to narcolepsy which is characterised by unpredictable transitions between wakefulness and sleep [31, 13].

Assuming that alterations of orexin levels are also controlling natural sleep-wake transitions, we have developed a novel concept of homeostatic sleep-wake regulation [47]. This concept has been transferred into a conductance-based model representing dynamics of neurons and synapses with activity-dependent decline of orexin effects during wakefulness and recovery during sleep. Implementing the experimentally well demonstrated projections from orexin neurons to the thalamus and modeling thalamic neurons as single neuron pattern generators, as in section 5.6, we have demonstrated alterations of thalamic synchronization states developing from changed orexin input. A brief preliminary report of this work has appeared in [48].

5.7.2 Modeling Hypothalamic Control of Thalamic Synchronization

For these simulations we need to connect neuronal populations of different brain areas. Nevertheless, we have continued with the conductance-based modeling approach, but with significant simplifications in other respect. The different neuronal populations are represented by single neurons connected via single synapses (Fig. 5.12A). This reduced modeling concept was chosen not for shortening the simulation time, which is often the main objection against conductance-based models. It

was chosen because our goal was to specifically examine the dynamics of synaptic plasticity in context with neuronal excitability. Averaged values from a large number of neurons or neuronal populations would complicate the study or may even prevent the elucidation of the physiological mechanisms at the cellular level.

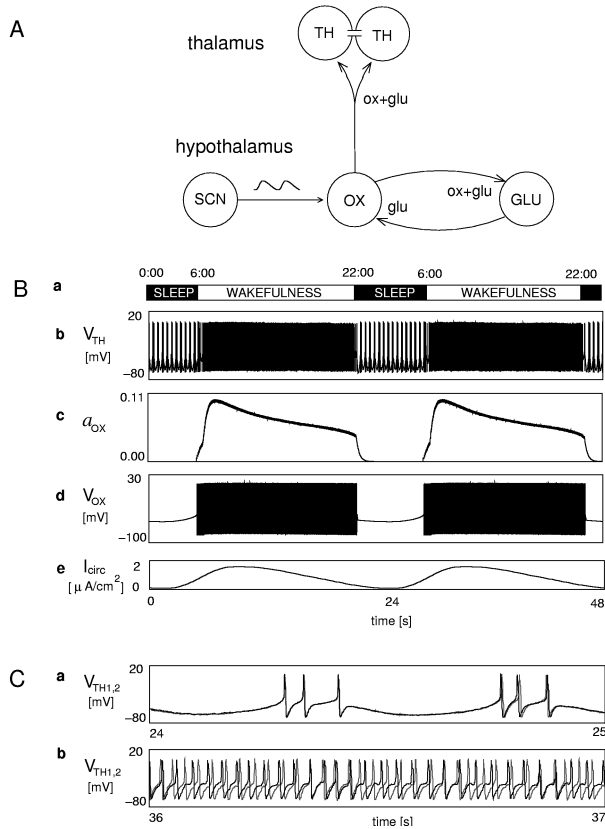


Fig. 5.12 A model of hypothalamic sleep-wake regulation controlling thalamic synchronization. A: Structure of the sleep-wake model consisting of a reciprocal excitatory circuit in the lateral hypothalamus with synaptic connections between an orexin (OX) and a local glutamate (GLU) neurons. The OX neuron receives circadian input from the suprachiasmatic nucleus (SCN) and sends synaptic projections to two gap-junction coupled thalamic neurons (TH). B: (a) Sleep-wake transitions along 24 h days and corresponding alterations of relevant model parameters on a 24 s time scale showing (b) voltage traces of a TH neuron with transitions from tonic firing to bursting, (c) the activation variable of synaptic orexin release, (d) transitions from silent to firing states of the OX neuron, and (e) the circadian input. C: Voltage traces of (a) synchronized bursting and (b) asynchronous tonic firing of the two thalamic neurons from the above simulations plotted on an enhanced time scale. Modified and merged from [47, 48].

In the core of the model, shown in Fig. 5.12A, there is a reciprocal excitatory circuit which is built up of an orexin neuron and a glutamate interneuron [30]. The

orexin neuron, which is a glutamate neuron with orexin as a co-transmitter, receives additional input from the circadian pacemaker in the form of a gradually changing current, corresponding to compound synaptic input from the SCN. Simulation of thalamic synchronization requires a minimum of two neurons. This simple network comprises all of the components of our conductance-based modeling approach:

1. Hypothalamic neurons are realized with the simplest version of a two-dimensional HH-type model - as described in section 5.4.
2. Thalamic neurons additionally include subthreshold currents allowing transitions between different types of impulse patterns - as illustrated in section 5.5.
3. Connections between the two thalamic neurons are made by gap-junctions with alterations of the synchronization state depending on the activity pattern - as shown in section 5.6.
4. Hypothalamic neurons make connections via chemical synapses which allow accounting for activity-dependent synaptic plasticity - as mentioned in section 5.7.

The dynamically relevant mechanisms of homeostatic sleep control are implemented via activity-dependent alterations of orexin effects. Firing of orexin neurons during wakefulness is only sustained by reciprocal excitatory connections, among others, with local glutamate interneurons [30]. The depolarizing effect of the co-transmitter orexin is obviously essential to keep them in an excitable state. To account for the transition to a silent sleep state, we have proposed an activity-dependent change of the synaptic efficacy of orexin, i.e., its reduction due to the firing of orexin neurons. This leads to an increasing sleep drive, similar to the enhanced tendency to falling asleep with lack of orexin in narcolepsy.

In the original model, the synapses have been implemented with additional simplifications compared to the model in Fig. 5.11, e.g., relating current activation directly to the transmitter concentration and distinguishing metabotropic orexin effects from ionotropic glutamate effects by longer time delays of activation and inactivation (for details see [47]). For consistency, we refer to the equations of Fig. 5.11 in the description of the state-dependent alterations of orexin effects, which have been introduced by a modulation function M scaling postsynaptic receptor and current activation, respectively:

$$\frac{da_r}{dt} = \frac{M \cdot p_r}{\tau_{act}} - \frac{a_r}{\tau_{inact}} \quad \text{with } 0 \leq M \leq 1 \quad (5.20)$$

$$\frac{dM}{dt} = \frac{M \cdot p_r}{\tau_{dec}} + \frac{M_{max} - M}{\tau_{inc}} \quad (5.21)$$

Alteration of M can reflect up- and down-regulation of postsynaptic receptors. Down-regulation, the first term in Eq. (5.20), depends on receptor occupation and is directly related to presynaptic firing and transmitter release. Up-regulation is implemented as an ongoing process of receptor re-embedding towards a maximum value M_{max} . In a similar way, activity-dependent depletion of presynaptic transmitter avail-

ability and its re-synthesis can be considered, with the time constants τ_{dec} and τ_{inc} determining the time scale on which M is decreasing and increasing, respectively.

To save computational time, most simulations as those in Fig. 5.12B and C were run with circadian cycle periods of 24 seconds instead of 24 hours. The homeostatic mechanisms can easily be scaled up to 24 hours multiplying the time constants τ_{dec} and τ_{inc} by a factor of 3600 (seconds/hour) as demonstrated in the original paper [47]. None of all the other parameters needs to be changed and, importantly, neuronal spike generation and synaptic transmission retain their realistic time-course.

The circadian input I_{circ} to the orexin neuron is modeled in form of the skewed sine function (Fig. 5.12Be) as proposed in [14]. At a certain input strength, the orexin neuron is activated. When the orexin neuron has reached a certain firing rate, it activates the glutamate interneuron - provided sufficiently strong contribution of the co-transmitter orexin. When this state is reached, firing in both neurons sustains due to their reciprocal excitation (Fig. 5.12Bd, illustrated by voltage trace of the orexin neuron, V_{ox}). The neurons continue to fire also when the circadian input decreases below the level of spike initiation or even without any input. When firing in the reciprocal circuit is established, it will only be interrupted by the impairment of synaptic transmission due to activity-dependent reduction of synaptic orexin effects as described above. When the postsynaptic efficacy a_{ox} (Fig. 5.12Bc) is going below a certain value, the orexin neuron cannot longer activate the glutamate neuron. The reciprocal excitation is interrupted, and firing stops. At this point, also the input from orexin neurons to the thalamic neurons is interrupted.

Thalamic neurons are modeled as pattern generators, like those in section 5.5, with synchronization properties, which are described in section 5.6. The excitatory synaptic input from the orexin neuron during wake keeps the thalamic neurons in a depolarized state with tonic firing activity which is only slightly changed by the decreasing activation variable. Absence of this depolarizing input during the silent state of the orexin neuron does not completely stops the firing of the thalamic neurons as in the case with the local glutamate interneuron. The thalamic neurons remain active, but the temporal pattern of impulse generation changes from tonic firing to bursting. These transitions are sufficient to bring the gap-junction coupled thalamic neurons from an asynchronous (Fig. 5.12Cb) to a synchronized state (Fig. 5.12Ca). This is exactly what could be expected from the intrinsic dynamics of thalamic neurons under the influence of external currents as described in section 5.6. And it exactly corresponds to the experimentally observed changes in thalamocortical circuits at the transitions from wakefulness to sleep [32, 35].

In this conclusive simulation section, we have combined our models of neuronal excitability, pattern generation, and synchronization with recently developed simulations of synaptic plasticity in homeostatic processes for an integrative approach connecting hypothalamic and thalamic systems of sleep-wake regulation. The connections were made between individual neurons with single synapses which likewise may represent a compound input from one brain nucleus to another. In this case, however, the relevant input is provided by the activation variable of postsynaptic receptors a_r . The amplitude and time-course of a_r depend not only on the synaptic strength but, due to the superposition of the postsynaptic currents, also on

the firing rate. In the reciprocal circuit, the firing rate essentially depends on the input from the other neuron and, in case of the orexin neuron, is additionally modulated by the circadian input. The activation variable itself is scaled as a function of the firing rate, i.e. transmitter or postsynaptic receptor occupation. Such complex interdependences can only be recognized with a conductance-based approach. They are developing from basic physiological processes and are of functional relevance for the model dynamics [47].

Acknowledgements SP acknowledges the support of Australian Research Council (ARC) and National Health and Medical Research Council (NHMRC). CF was supported by grant FE359/10 of the German Science Foundation (DFG). The authors thank Dr. Kurt Mandrek for valuable discussion of the Hodgkin-Huxley approach to neuronal modeling.

References

1. Amzica F, Steriade M (1998) Electrophysiological correlates of sleep delta waves, *Electroencephalogr Clin Neurophysiol* 107:69-83.
2. Bazhenov M, Timofeev I, Steriade M, Sejnowski T J (2002) Model of thalamocortical slow-wave sleep oscillations and transitions to activated States, *J Neurosci* 22:8691-8704.
3. Blumenfeld H and McCormick D A (2000) Corticothalamic inputs control the pattern of activity generated in thalamocortical networks, *J Neurosci* 20:5153-5162.
4. Borbely A A (1982) A two process model of sleep regulation, *Hum Neurobiol* 1:195-204.
5. Braun H A, Bade H, Hensel H (1980) Static and dynamic discharge patterns of bursting cold fibers related to hypothetical receptor mechanisms, *Pflugers Arch* 386:1-9.
6. Braun H A, Dewald M, Schäfer K, Voigt K, Pei X, Dolan K, Moss F (1999) Low-dimensional dynamics in sensory biology 2: facial cold receptors of the rat, *J Comput Neurosci* 7:17-32.
7. Braun H A, Schäfer K, Voigt K, Huber M T (2003a) Temperature encoding in peripheral cold receptors: Oscillations, resonances, chaos and noise, *Nova Acta Leopoldina NF* 88:293-318.
8. Braun H A, Voigt K, Huber M T (2003b) Oscillations, resonances and noise: basis of flexible neuronal pattern generation, *Biosystems* 71:39-50.
9. Braun H A, Wissing H, Schaafer K, Hirsch M C (1994) Oscillation and noise determine signal transduction in shark multimodal sensory cells, *Nature* 367:270-273.
10. Blumberger D M, Daskalakis Z J, Mulsant B H (2008) Biomarkers in geriatric psychiatry: searching for the holy grail? *Curr Opin Psychiatry* 21:533-539.
11. Burns R S, Chiueh C C, Markey S P, Ebert M H, Jacobowitz D M, Kopin I J (1983) A primate model of parkinsonism: selective destruction of dopaminergic neurons in the pars compacta of the substantia nigra by N-methyl-4-phenyl-1,2,3,6-tetrahydropyridine, *Proc Natl Acad Sci U S A* 80:4546-4550.
12. Carlsson A, Carlsson M L (2006) A dopaminergic deficit hypothesis of schizophrenia: the path to discovery, *Dialogues Clin Neurosci* 8:137-142.
13. Chemelli R M, Willie J T, Sinton C M, Elmquist J K, Scammell T, Lee C, Richardson J A, Williams S C, Xiong Y, Kisanuki Y, et al., (1999) Narcolepsy in orexin knockout mice: molecular genetics of sleep regulation, *Cell* 98:437-451.
14. Daan S, Beersma D G, Borbely A A (1984) Timing of human sleep: recovery process gated by a circadian pacemaker, *Am J Physiol* 246:R161-R178.
15. Fambrough D M, Drachman D B, Satyamurti S (1973) Neuromuscular junction in myasthenia gravis: decreased acetylcholine receptors, *Science* 182:293-295.
16. Finke C, Freund J A, Rosa E Jr, Braun H A, Feudel U (2010) On the role of subthreshold currents in the Huber-Braun cold receptor model, *Chaos* 20:045107- 045107-11.

17. Finke C, Postnova S, Rosa E, Freund J A, Huber M T, Voigt K, Moss F E, Braun H A, Feudel U (2010) Noisy activation kinetics induces bursting in the Huber-Braun neuron model, *Eur Phys J-ST* 187:199-203.
18. Finke C, Vollmer J, Postnova S, Braun H A (2008) Propagation effects of current and conductance noise in a model neuron with subthreshold oscillations, *Math Biosci* 214:109-21.
19. FitzHugh R (1961) Impulses and physiological states in theoretical models of nerve membrane, *Biophysical J* 1:445-466.
20. Hauptmann C, Roulet J C, Niederhauser J J, Döll W, Kirlangic M E, Lysyansky B, Krachkovskiy V, Bhatti M A, Barnikol U B, Sasse L, Bührle C P, Speckmann E J, Götz M, Sturm V, Freund H J, Schnell U, Tass P A (2009) External trial deep brain stimulation device for the application of desynchronizing stimulation techniques, *J Neural Eng* 6:066003.
21. Hill S and Tononi G (2005) Modeling sleep and wakefulness in the thalamocortical system, *J Neurophysiol* 93:1671-1698.
22. Hindmarsh J L, Rose R M (1982) A model of the nerve impulse using two first-order differential equations, *Nature* 296:162-164.
23. Hodgkin A L and Huxley A F (1952) A quantitative description of membrane current and its application to conduction and excitation in nerve, *J Physiol* 17:500-544.
24. Huber M T and Braun H A (2006) Stimulus-response curves of a neuronal model for noisy subthreshold oscillations and related spike generation, *Phys Rev E Stat Nonlin Soft Matter Phys* 73:041929.
25. Huber M T, Krieg J C, Dewald M, Voigt K, Braun H A (1998) Stimulus sensitivity and neuromodulatory properties of noisy intrinsic neuronal oscillators, *Biosystems* 48:95-104.
26. Jin W, Postnova S, Braun H A (2011) Stochastic Resonance and Stochastic Encoding: Cooperative Effects of Noise and Intrinsic Dynamics in a Model Neuron with Subthreshold Oscillations, In: Wang R and Gu F (eds) *Advances in Cognitive Neurodynamics (II)*, Springer.
27. Lee M G, Hassani O K, Jones B E (2005) Discharge of identified orexin/hypocretin neurons across the sleep-waking cycle, *J Neurosci* 25:6716-6720.
28. Leloup J C and Goldbeter A (2003) Toward a detailed computational model for the mammalian circadian clock, *Proc Natl Acad Sci U S A* 100:7051-7056.
29. Levy R (2000) High-frequency synchronization of neuronal activity in the subthalamic nucleus of parkinsonian patients with limb tremor, *J Neurosci* 20:7766-7775.
30. Li Y, Gao X B, Sakurai T, van den Pol A N (2002) Hypocretin/orexin excites hypocretin neurons via a local glutamate neuron-A potential mechanism for orchestrating the hypothalamic arousal system, *Neuron* 36:1169-1181.
31. Lin L, Faraco J, Li R, Kadotani H, Rogers W, Lin X, Qiu X, de Jong P J, Nishino S, and Mignot E (1999) The sleep disorder canine narcolepsy is caused by a mutation in the hypocretin (orexin) receptor 2 gene, *Cell* 98:365-376.
32. Llinas R R and Steriade M (2006) Bursting of thalamic neurons and states of vigilance, *J Neurophysiol* 95:3297-308.
33. Lu J, Sherman D, Devor M, Saper C B (2006) A putative flip-flop switch for control of REM sleep, *Nature* 441:589-594.
34. McCormick D A (2002) Cortical and subcortical generators of normal and abnormal rhythmicity, *Int Rev Neurobiol* 49:99-114.
35. McCormick D A and Feeseer H R (1990) Functional implications of burst firing and single spike activity in lateral geniculate relay neurons, *Neuroscience* 39:103-113.
36. Mileykovskiy B Y, Kiyashchenko L I, Siegel J M (2005) Behavioral correlates of activity in identified hypocretin/orexin neurons, *Neuron* 46:787-798.
37. Modolo J, Mosekilde E, Beuter A (2007) New insights offered by a computational model of deep brain stimulation, *J Physiol Paris* 101:56-63.
38. Mormann F, Kreuz T, Andrzejak R G, David P, Lehnertz K, Elger C E (2003) Epileptic seizures are preceded by a decrease in synchronization, *Epilepsy Res* 53:173-185.
39. Morris C and Lecar H (1981) Voltage oscillations in the barnacle giant muscle fiber, *Biophys J* 35:193-213.
40. Noble D (1962) A modification of the Hodgkin-Huxley equations applicable to Purkinje fibre action and pace-maker potentials, *J Physiol* 160:317-352.

41. Noble D (2004) Modeling the heart, *Physiology (Bethesda)* 19:191-197.
42. Noori H R and Jaeger W (2010) Neurochemical oscillations in the basal ganglia, *Bull Math Biol* 72:133-147.
43. Phillips A J K and Robinson P A (2007) A quantitative model of sleep-wake dynamics based on the physiology of the brainstem ascending arousal system, *J Biol Rhythms* 22:167-179.
44. Postnova S, Finke C, Jin W, Schneider H, Braun H A (2010) A computational study of the interdependencies between neuronal impulse pattern, noise effects and synchronization, *J Physiol Paris* 104:176-189.
45. Postnova S, Rosa E Jr, Braun H A (2010) Neurones and synapses for systemic models of psychiatric disorders, *Pharmacopsychiatry* 43:S82-S91.
46. Postnova S, Voigt K, Braun H A (2007b) Neural synchronization at tonic-to-bursting transitions, *J Biol Phys* 33:129-143.
47. Postnova S, Voigt K, Braun H A (2009) A mathematical model of homeostatic regulation of sleep-wake cycles by hypocretin/orexin, *J Biol Rhythms* 24:523-535.
48. Postnova S, Voigt K, Braun H A (2011) Modelling the Hypothalamic Control of Thalamic Synchronization along the Sleep-Wake Cycles, in: Wang R and Gu F (eds.) *Advances in Cognitive Neurodynamics (II)*, Springer.
49. Postnova S, Wollweber B, Voigt K, Braun H A (2007) Impulse pattern in bi-directionally coupled model neurons of different dynamics, *Biosystems* 89:135-142.
50. Qi Z, Miller G W, Voit E O (2010) Computational modeling of synaptic neurotransmission as a tool for assessing dopamine hypotheses of schizophrenia, *Pharmacopsychiatry* 43:S50-S60.
51. Rinzel J (1975) Spatial stability of traveling wave solutions of a nerve conduction equation, *Biophys J* 15:975-988.
52. Robinson P A, Rennie C J, Rowe D L, O'Connor S C, Gordon E (2005) Multiscale brain modeling, *Philos Trans R Soc Lond B Biol Sci* 360:1043-1050.
53. Saper C B, Fuller P M, Pedersen N P, Lu J, Scammell T E (2010) Sleep state switching, *Neuron* 68:1023-1042.
54. Schaefer K, Braun H A, Isenberg C (1986) Effect of menthol on cold receptor activity. Analysis of receptor processes, *J Gen Physiol* 88:757-776.
55. Schäfer K, Braun H A, Rempe L (1991) Discharge pattern analysis suggests existence of a low-threshold calcium channel in cold receptors, *Experientia* 47:47-50.
56. Sherin J E, Shiromani P J, McCarley R W, Saper C B (1996) Activation of ventrolateral preoptic neurons during sleep, *Science* 271:216-219.
57. Singer W (1993) Synchronization of cortical activity and its putative role in information processing and learning, *Annu Rev Physiol* 5:349-374.
58. Schmidt H D and Pierce R C (2010) Cocaine-induced neuroadaptations in glutamate transmission: potential therapeutic targets for craving and addiction, *Ann N Y Acad Sci* 1187:35-75.
59. Sutcliffe J G and de Lecea L (2002) The hypocretins: setting the arousal threshold, *Nat Rev Neurosci* 3:339-349.
60. Tessone C J, Mirasso C R, Toral R, Gunton J D (2006) Diversity-induced resonance, *Phys Rev Lett* 97:194101.
61. Tononi G and Cirelli C (2006) Sleep function and synaptic homeostasis, *Sleep Med Rev* 10:49-62.
62. Tsujino N and Sakurai T (2009) Orexin/Hypocretin: A neuropeptide at the interface of sleep, energy homeostasis, and reward system, *Pharmacol Rev* 61:162-176.
63. Westerhoff H V, Kolodkin A, Conradie R, Wilkinson S J, Bruggeman F J, Krab K, van Schuppen J H, Hardin H, Bakker B M, Moné M J, Rybakova K N, Eijken M, van Leeuwen H J, Snoep J L (2009) Systems biology towards life in silico: mathematics of the control of living cells, *J Math Biol* 58:7-34.
64. Williams J W Jr, Mulrow C D, Chiquette E, Noël P H, Aguilar C, Cornell J (2000) A systematic review of newer pharmacotherapies for depression in adults: evidence report summary, *Ann Intern Med* 132:743-756.